Scientific Research Journal,
Vol 22, No 1 (2025) 101-124
https://doi.org/10.24191/srj.v22i1.17033

Properties of Magnesium-Zinc Graphene Composites

Nur Maizatul Shima Adzali[1,*], Nur Hidayah Ahmad Zaidi[1], Saidatulakmar Shamsuddin[2], Muhamad Ielman Irsyaduddin Mohd Zahferee[2], Muhammad Najmi Mohammad Zamri[2], Irfan Shariq Saidan[2], Nurul Amira Kushairi[2]

[1]Faculty of Chemical Engineering and Technology, Kompleks Pusat Pengajian Jejawi 3, Kawasan Perindustrian Jejawi, Universiti Malaysia Perlis (UniMAP), 02600 Arau, Perlis
[2]Faculty of Applied Sciences, Universiti Teknologi MARA, 02600 Arau, Perlis.

[*]Corresponding Author's E-mail: shima@unimap.edu.my

Received: 12 December 2024
Accepted: 12 January 2025
Online First: 01 March 2025

ABSTRACT

Magnesium (Mg) is a metal that is light in weight and well known for its high strength to various role in several biological processes, automotive components, alloys, and aerospace applications. The purpose of this study is to fabricate and determine the physical and mechanical properties of Mg-Zn reinforced with graphene composites, with concern for enhancement of super strong material made of carbon atoms. The focus is on figuring out the effect of different percentages of graphene on the physical and mechanical properties of the composite. The aim of this research is to identify the best ratio that gives the hard and most durable Mg-Zn composite by using hardness test, Archimedes test, and XRD analysis. Five sample of Mg- Zn were fabricated with different percentages of graphene which were 0 wt.%, 1 wt.%, 3 wt.%, 5 wt.%, and 7 wt.%. All 5 samples were mixed in mixing drum for 30 minutes with speed of 200 revolutions per minute then the mixture is then placed in mold and compressed for 2 minutes under 8 tons of hydraulic pressure. Then the sample undergo sintering process where it was sintered for 2 hours in 350 °C. Then the sample were ground and polished before undergo hardness, Archimedes, and XRD test. Hardness result for Mg-Zn reinforced with graphene shows that the highest hardness value is with addition 3 wt.% of graphene (53.93 HRF), while the lowest reading is for 0 wt.% of graphene (26.67 HRF). For density result, maximum relative density (91.08%), was obtained from graphene percentage at 3 wt.%, while the lowest relative density (82.37%), was obtained from graphene

percentage at 0 wt.%. From this research, sample with 3 wt.% of graphene shows better properties in term of hardness, porosity and XRD analysis. To conclude, the present work showed a successful fabrication of Mg-Zn composite added with graphene for application in biomedical sector and other sector.

Keywords: Magnesium; Zinc; Alloy; Powder Metallurgy (PM); Graphene

INTRODUCTION

Growing demand for lightweight, high-performing materials in many kinds of industrial applications has made the development of advanced materials a crucial field of study in recent years. Within these materials, magnesium (Mg) alloys have drawn a lot of interest because of their exceptional mechanical qualities, low density, and prospective application in lightweight components and structures making them suitable for used for medicinal purposes, automotive, and aerospace sectors. Because of its elastic modulus that is similar to the bone found naturally in the human body and its high biocompatibility, magnesium is a good material to use in implants. Inorganic stage crystals containing calcium are implanted in an organic natural stage that makes up bone, which is an exacerbated normal living tissue. It is acknowledged that resorption and disease cause bone tissue to shatter. Devices for fixing and obsessing over bones are made of metal and are used in healthcare settings [1]. Meanwhile, Zinc (Zn) is a very useful metal that is used to make die-cast items like door handles, galvanized steel for use in cars and construction, and alloys like brass and bronze that are used to make machine parts and plumbing fittings, respectively. Zinc is also needed to make zinc oxide, which is an essential component of paint, rubber, and other items, as well as zinc batteries. The fact that zinc is widely used confirms its importance in a variety of industrial sectors.

Because of its special qualities in heat conductivity, lubrication, and mechanical performance, graphene is mostly applied to many different industries [2]. Graphene has an elastic modulus of 1100 GPa and a tensile strength of 125 GPa and research indicates that the strength and ductility of pure magnesium can be enhanced by adding more reinforcement like graphene [3]. Typically, the reinforcements utilized in the composites are

powders and graphene is an efficient choice for the reinforcement in metal matrix composites to achieve the highest level of perfect conductivity and superior mechanical qualities [1]. A single sheet of graphite has garnered significant attention because of its exceptional mechanical, thermal, and electrical characteristics. Thermally conductive nanomaterials like graphene have shown to be good fillers in the field of thermal interface materials (TIMs). In this study, graphene is used because it is incredibly strong, light, and has good thermal and electrical conductivity. It also increases the strength, toughness, and adaptability of materials for a variety of applications, and has special qualities such as its incompatibility with the body and ability to block the passage of gases, makes it useful for the development of cutting-edge materials [4]. Few layer graphene, or graphene nanoplatelets, has also been proposed as the perfect reinforcement to enhance the mechanical and electrical properties of various polymers [5]. An effort was made in 2011 to use hot isostatic pressing and extrusion procedures to create the Al-graphene nanocomposite. According to the experimental findings, the Al-graphene nanocomposite's strength and hardness had reduced [6].

Preliminary studies show the magnesium metal composite made by vacuum hot press sintering, which contains nickel coated graphene nanoplatelets [7]. According to their findings, the graphene nanoplatelets are uniformly distributed throughout the matrix and exhibit a 35% improvement in hardness and compressive strength when compared to the base material. When compared to the base material, the composite also had a lower wear rate [1]. Xiang *et al.* [8] studied the multi-step dispersion process for graphene nanoplatelets reinforced magnesium metal matrix composites. According to their findings, the mechanical qualities such as tensile strength and hardness steadily rise with an increase in graphene nanoparticles. Their research demonstrates a cutting-edge method for adding graphene nanoparticles to metals [8].

The main goal of the present research is to apply the powder metallurgy method to fabricate Mg-Zn matrix composites that are reinforced with graphene. Fabrication technique by using powder metallurgy technique offers many advantages includes minimized waste materials & costs, ability to alter final properties and also producing precise and complex parts. The study of advanced techniques is motivated by the need for lightweight,

high-performance materials. Magnesium-Zinc alloys complement versatile zinc in a variety of sectors. They are valued for their mechanical strength and uses in aerospace, automotive, and medical. Graphene, recognized for its strength and heat conductivity, improves materials even more. Together, they meet the demand for effective solutions across many industries.

EXPERIMENTAL METHODOLOGY

Description of Method

This experiment employed the powder metallurgy method (PM) to synthesize a composite material comprising magnesium-zinc (Mg-Zn) reinforced with graphene. In contrast to traditional methods such as casting, forging, or extrusion, PM had stood out for its heightened versatility, notably enhancing thermal properties, interfacial bonding strength, and microstructure. This distinction was particularly salient when the researchers used PM for the reinforcement of magnesium with graphene, utilizing both the powder metallurgy method and sintering in a vacuum atmosphere. For creating complex-shaped parts with high surface polish and dimensional precision, it had been affordable and straightforward to process. The PM process had a number of benefits, such as the ability to produce finished goods with the required exact tolerance and surface quality, the ability to reduce or even completely eliminate machining traditionally applied in manufacturing, and the reduction of scrap losses through the reduction or elimination of chip removal. The choice of powder depended on what the produced component required. The manufacturing flowchart for powder metallurgy had been divided into several steps.

Sample Preparation

Calculations were made for each metal material to determine its exact weight, the quantity of green samples to be produced, and the appropriate size for compression. Magnesium powder (78 wt.%, 77 wt.%, 75 wt.%, 73 wt.%, and 71 wt.%), zinc powder (20 wt.%), and graphite powder (1 wt.%, 3 wt.%, 5 wt.% and 7 wt.%) were mixed with stearic acid (2 wt.%). Table 1 lists the quantity of each raw metal ingredient.

Table 1: The weight for each raw material used.

	Magnesium	Zinc	Graphene	Stearic Acid	Total
Sample 1	1.56 g (78%)	0.4 g (20%)	0.00 g (0%)	0.04 g (2%)	2.0 g
Sample 2	1.54 g (77%)	0.4 g (20%)	0.02 g (1%)	0.04 g (2%)	2.0 g
Sample 3	1.50 g (75%)	0.4 g (20%)	0.06 g (3%)	0.04 g (2%)	2.0 g
Sample 4	1.46 g (73%)	0.4 g (20%)	0.10 g (5%)	0.04 g (2%)	2.0 g
Sample 5	1.42 g (71%)	0.4 g (20%)	0.14 g (7%)	0.04 g (2%)	2.0 g

Mixing

The first stage in the powder metallurgy (PM) process involved mixing. Each container held a mixture of magnesium, zinc, graphite, and stearic acid powders. The containers were placed on a spinning mixing drum and rotated at a speed of 200 revolutions per minute (rpm) for 30 minutes in a milling machine to achieve a good distribution of the mixture.

Compacting

After the mixing process, the metal powder mixture of magnesium, zinc, graphite, and stearic acid was inserted into the mold for the compacting process. The mixture was then pressed into the desired shape using a hydraulic press at 8 tons. The compacted samples were left to rest for 2 minutes. Before compacting, the weight of the mixed composite was measured to ensure it was 2 grams. There are two main pressing techniques: hot pressing and cold pressing. Cold pressing was chosen for this study due to the use of a hydraulic press. The resulting product was referred to as a "green sample," and five samples were created in this process. After all the samples underwent the process, their diameter and thickness were measured using a digital caliper.

Sintering

The green samples underwent the sintering process in a muffle furnace. The compressed products were heated during sintering to a temperature slightly below their melting point. This procedure facilitated the particles' ability to bind and form a solid mass. The green samples were heated to 350 °C for two hours. A heating rate of 5 °C/min was used for one hour of

heating. After completing the sintering process, the sintered parts were left to cool. The final step involved grinding to achieve the desired dimensional tolerance (closest final shape) and the required mechanical and physical properties. The samples were then placed in a desiccator containing silica gel to prevent oxidation. Figure 1 shows sintering profile for the samples, which have been sintered at 350 °C.

Figure 1: Graph of sintering profile at 350 °C.

Grinding

The metallographic technique, a series of procedures used in materials science, metallurgy, and engineering to investigate the characteristics and behaviors of metallic materials, was employed. This technique involves preparing, examining, and analyzing the microstructure of the materials. As part of this process, a thin, polished sample was created to study its internal structure, phases, inclusions, grain boundaries, and other microstructural features under a microscope.

The sintered samples were then ground using various grits of sandpaper. The grinding process started with the roughest grit, 240, and progressed to finer grits of 320, 400, 500, 600, 800, 1000, and finally 1500, achieving a smooth finish. A grinding and polishing machine was used for this process. The samples were ground at 100 rpm for 2 minutes to avoid over-grinding, which can cause various problems. Excessive grinding can generate heat that may degrade the samples or induce unwanted chemical reactions that alter their composition.

Polishing

The samples were then polished using diamond paste with grits of 6 microns, 3 microns, and 1 micron, applied in succession. Powder metallurgy components that had undergone compaction and sintering processes often have uneven or rough surfaces. Polishing was therefore necessary to improve the surface finish of these components. Polishing creates a smoother and more aesthetically pleasing surface by removing imperfections such as holes, voids, and roughness. This is particularly important for components with a significant visual impact, such as auto parts, consumer goods, or medical equipment. Additionally, polishing can reduce surface imperfections like microcracks and voids that act as stress concentrators and weaken the component. It can also be used to enhance the mechanical properties of powder metallurgy components. By removing these flaws, polishing can improve strength, fatigue resistance, and overall mechanical performance. Finally, polishing aids in cleaning the surface of powder metallurgy components by removing any remaining impurities or oxides that may have formed during the manufacturing process. The samples were first washed with distilled water to remove surface impurities, followed by the application of ethanol to remove water stains.

XRD Test (X-Ray Diffraction test)

X-ray diffraction (brand XRD-600 Shimadzu) was used to analyze the structure of a composite sample made of magnesium-zinc reinforced with graphene. XRD is a powerful analytical technique that utilizes the diffraction pattern created by the scattering of X-rays by a crystal's atoms. This pattern reveals information about the crystal structure and behavior of crystalline materials.

For the analysis, a composite sample was prepared, typically in the form of a bulk material or a thin film. The sample was then exposed to X-ray radiation. By analyzing the resulting diffraction pattern, researchers were able to determine the structural characteristics, phase composition, crystallographic orientation, and any interactions between the magnesium-zinc and graphene within the composite material. The elements present in the sample were identified using the XRD machine and their data displayed in the HighScore Plus application.

Archimedes Test

This experiment employed Archimedes' principle to determine the density and porosity of the sintered samples, using both the base metal and the reinforcement material. The density measurement procedure involved weighing the samples in both air and a fluid with a known density. Densimeters were used to determine the sample densities, and the weight of the submerged sample was measured. Archimedes' principle, a fundamental concept in physics, states that the buoyant force experienced by an object immersed in a fluid is equal to the weight of the fluid displaced by the object. This principle describes the behavior of objects submerged in fluids. The relative density and bulk density were then calculated using Equation (1) and Equation (2).

$$\text{Relative Density}(\%) = (\text{Bulk density}) / (\text{Theoretical}) \times \text{Density of water}) \quad (1)$$

$$\text{Bulk Density}, \rho = W_a / (W_c - W_b) \times \text{Density of water}) \quad (2)$$

W_a = weight of sample in air (g)
W_b = apparent weight of sample (g)
W_c = saturated weight of sample (g)

The theoretical density, ρ_T was calculated using Equation (3).

$$\rho_T = \rho_{Mg}(78\text{wt.}\%) + \rho_{Zn}(20\text{wt.}\%) + \rho_{graphene}(2\text{wt.}\%) \quad (3)$$

The porosity of the sample was calculated using Equation (4).

$$\text{Total Porosity}(\%) = 100\% - \text{Relative density } (100\%) \quad (4)$$

Rockwell Hardness Test

This study employed Rockwell hardness testing, a widely used method for measuring the hardness of materials, particularly metals. The test reveals how far an indenter penetrates a material under a specific load, providing insight into a metal's response to heat and mechanical treatments. For this investigation, a 1/16 conical diamond indenter was used with a minimal applied force. The Rockwell hardness value is expressed as a number on the Rockwell scale. In the forthcoming Rockwell hardness test, a systematic procedure will be followed to determine the hardness of a material.

Optical Microscope

An optical microscope (OM) was employed to examine the microstructure of the samples. Metallographic analysis was conducted using an optical microscope. This technique allows visualization and magnification of tiny samples or objects invisible to the naked eye. Polished cross-sectional or surface samples were prepared for examination under the optical microscope. These specimens were positioned on the microscope stage and exposed to visible light. The resulting image, viewed through an eyepiece or captured by a camera, enabled magnified observation of the composite's microstructure. This included investigating and characterizing the distribution and interaction of magnesium-zinc and graphene within the material. In this investigation, a magnification of 100x was used on the OM. For metallographic analysis, an upward-facing light source was necessary. A downward-facing light source would render the sample unclear and obscure the structure.

RESULTS AND DISCUSSION

Raw Material Characterization

Magnesium (Mg) Powder

The particle size of Mg has been determined using the particle size analyser. Mg powder has a molar mass of 24.31 g/mol with density 1.738 g/cm^3. According to data from particle analyser, particle sizes are 50.122 µm at d (0.1), 120.52 µm at d (0.5), and 185.793 µm at d (0.9). Accordingly, 10% of the sample had a size lower than 50.122 µm, 50% is less than 120.52 µm, while 90% is less than 185.793 µm. When d (0.9) / d (0.1) is more than 1, it indicates a big distribution. Next, the volume distribution based on a RI value of 1.330 for the dispersant water and the particle sizes of this magnesium powder vary from 0.020 µm to 206.500 µm. Additionally, the span is 1.126 and the specific surface area of this magnesium powder is 0.0687 m^2/g.

Zinc (Zn) Powder

Analysis of Zn powder showed that its particle sizes are 28.546 um at d (0.9), 12.804 um at d (0.5), and 5.993 um at d (0.1). The molar mass

of Zn Powder is 65.4 g/mol, the density of Zn is about 7.13g/cm³, while the range analysis particle size of Zn powder is < 45um. According to data from particle analyser, a specific surface area of 0.595 m²/g is obtained. The particle size ranges from 0.020 µm to 206.500 µm, and the volume distribution, determined by the dispersant water's RI value of 1.330, is identical to that of the magnesium powder. 1.761 is the span that represents the distribution width. The model's volume ranges from 10% to 11%.

Graphite Powder

According to the results data, the particle sizes for graphite powder (graphene) are 10.368 µm at d (0.l), 35.052 µm at d (0.5), and 87.543 µm at d (0.9). The specific surface area of this graphite powder is 0.292 m²/g. The dispersant water's RI value of 1.330 corresponds to the volume distribution of the powdered magnesium and zinc, while the particle size ranges from 0.020 µm to 206.500 µm with there is a 2.202 span.

Fabrication of Mg-Zn Alloy Reinforced with Graphene

Figure 2 shows all the composites after has been sintered at 350 °C for all 5 various of graphene percentage which is 0 wt.%, 1 wt.%, 3 wt.%, 5 wt.%, and 7 wt.%. This demonstrated that the first objective had been accomplished to effectively use powder metallurgy to create composite materials that use magnesium-zinc (Mg-Zn) alloy matrix composites reinforce graphene [9]. This approach offers the potential to enhance the mechanical of the resulting composites. The sample has been prepared for 3 set to control for sample lost.

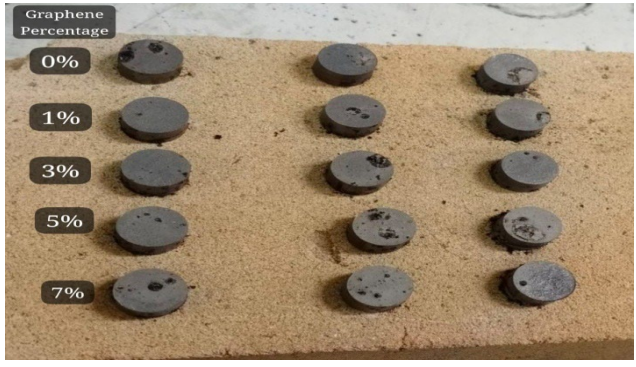

Figure 2: Fabrication of Mg-Zn alloy reinforced with graphene.

XRD Analysis

The XRD analysis, performed using HighScore Plus software with the COD database, identified the chemical elements present in the Mg-Zn alloy reinforced graphene samples with 3 wt.% and 7 wt.% graphene contents. Figure 3 shows raw XRD analysis comparison for percentage of graphene for sample 3 wt.% and 7 wt.%. Meanwhile, Figure 4 shows graph of XRD analysis for percentage of graphene for sample 3 wt.% and Figure 5 shows graph of XRD analysis for percentage of graphene for sample 7 wt.% that had been analysed. The results showed that the fabricated samples contained the correct elements, aligning with the research study.

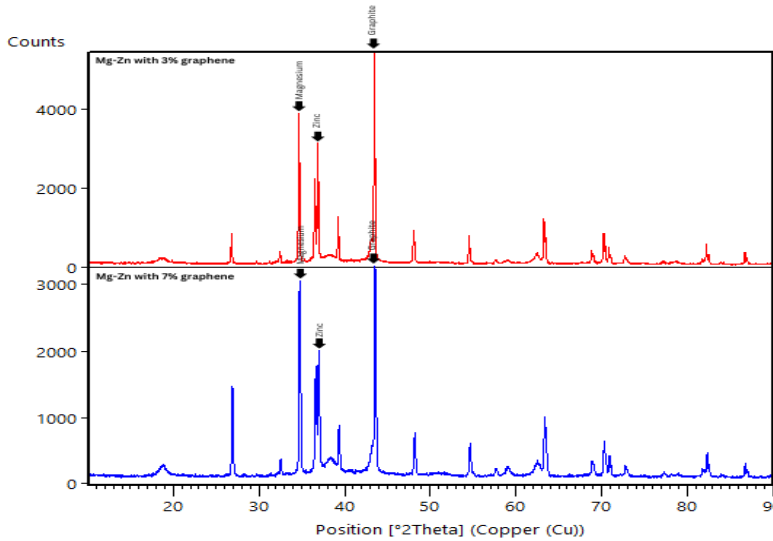

Figure 3: XRD analysis for percentage of graphene 3 wt.% and 7 wt. %.

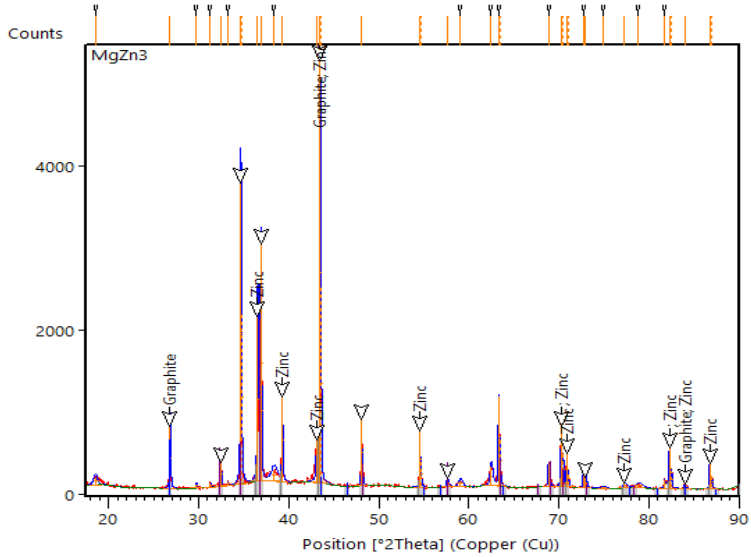

Figure 4: Graph of XRD analysis for percentage of graphene for sample 3 wt. %.

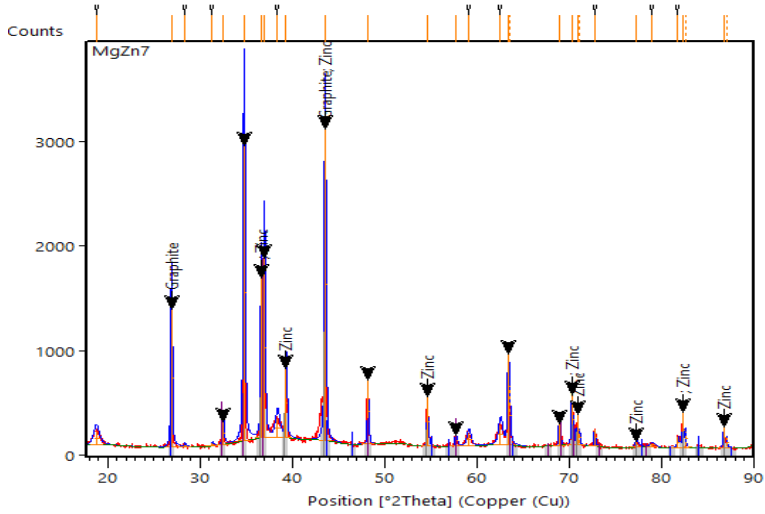

Figure 5: Graph of XRD analysis for percentage of graphene for sample 7 wt.%.

According to Figure 6 and 7, graphite was found to be the most element, appeared in 22 peaks for both samples. Zinc appeared to be the least element, with only 4 peaks for both samples. Magnesium, the second most element, appearing in 15 peaks for the 3 wt.% graphene sample and 14 peaks for the 7 wt.% graphene sample, according to the reference pattern. The XRD analysis also provided information about the crystal structures and lattice constants of the elements present in the composite. For Magnesium (Mg), it has hexagonal closed packed structure with lattice constants of 3.1940 Å (a and b-axis) and 5.1720 Å (c-axis) for both 3% and 7% graphene samples. Next, for Zinc (Zn) it has hexagonal structure with lattice constants of 2.6650 Å for both a and b-axis and 4.9470 Å for c-axis for the 3 wt.% graphene sample, and 2.6590 Å for both a and b-axis and 4.9370 Å for c-axis for the 7% graphene sample. Lastly, for Graphite, it has hexagonal structure with lattice constants of 2.4561 Å (a and b-axis) and 10.0410 Å for c-axis for both 3 wt.% and 7 wt.% graphene samples.

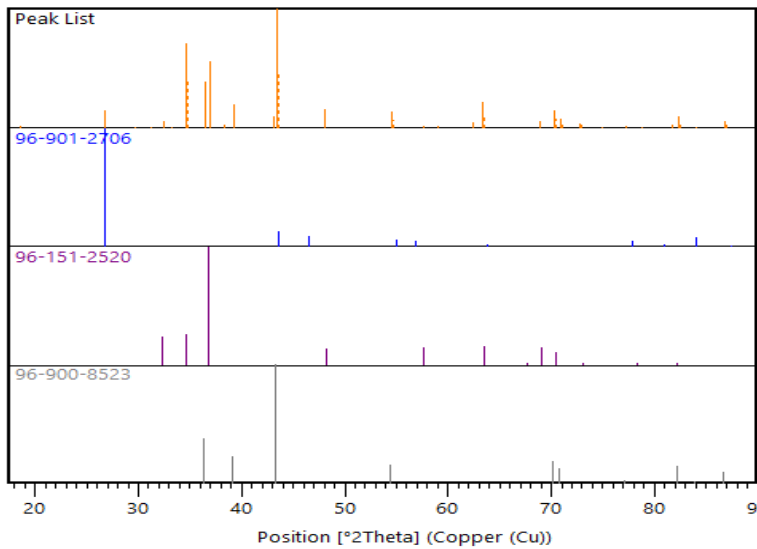

Figure 6: Comparison of peak list with peak of Mg, Zn and graphite for percentage of graphene for sample 3 wt.%.

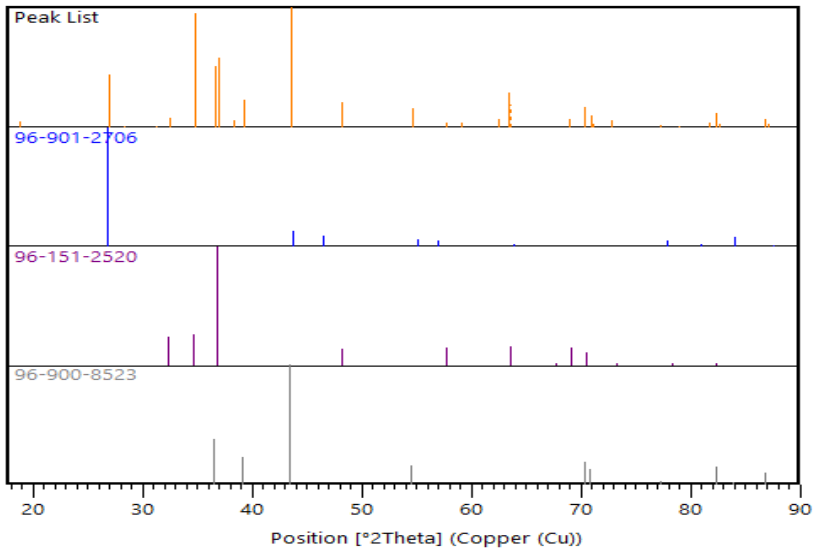

Figure 7: Comparison of peak list with peak of Mg, Zn and graphite for percentage of graphene for sample 7 wt.%.

The XRD results provide a visual representation of the peaks for Mg, Zn, and graphite, allowing for a comparison between the 3 wt.% and 7 wt.% graphene samples. Additionally, some outside elements, such as acetone, periclase, brucite, zincite, and pentacene, were found to be interfering with the XRD scan results. The XRD analysis of Mg-Zn alloy reinforced graphene confirms the successful integration of Mg-Zn alloy matrix with graphene. The presence of Mg, Zn, and graphite peaks in the diffraction pattern indicates that the composite material was successfully fabricated. The findings contribute to the understanding of the structural properties of the composite material and how these elements interact using the powder metallurgy method, advancing the knowledge of composite materials that offering stronger and more durable options, allowing for maximized functioning and further research on Mg-Zn alloy reinforced graphene composites for specific applications.

Density

In this study, Equation (1) was used to determine the relative density (%). However, bulk density needs to be determined before the relative

density can be obtained. Therefore, Equation (2) was used for determining the bulk density. This Mg-Zn alloy reinforced graphene has a theoretical density, p_T, of 2.40334 g/cm³, which was determined using Equation (3). A dimensionless measure used to compare the densities of reference substances is called relative density, sometimes referred to as specific gravity. It is frequently used to describe a material's buoyancy and density in various settings. The weight of the sample in dry condition is tabulated in Table 2.

Table 2: The weight of Mg-Zn sample with vary percentage of graphene.

Sample	Graphene (wt.%)	Dry weight (g)
1	0	1.92
2	1	1.86
3	3	1.89
4	5	1.87
5	7	1.86

Table 3 shows that the maximum relative density, 91.08%, was obtained from graphene percentage at 3 wt.%, while the lowest relative density, 82.37%, was obtained from graphene percentage at 0 wt.%. With reference to Figure 8, the graph illustrates a tendency towards increasing relative density as graphene percentage rises to 3 wt.% and then decreases at 5 wt.% and 7 wt.% of graphene. It shows that the sample is denser than samples at other percentage of graphene when the relative density achieves its maximum value at an ideal graphene proportion of 3%.

Table 3: The bulk density and relative density of Mg-Zn sample with vary percentage of graphene.

Sample	Graphene (wt.%)	Bulk density (g/cm³)				Relative Density (%)
		1	2	3	Average	
1	0	1.703	2.128	2.125	1.985	82.37
2	1	1.992	2.047	2.060	2.033	84.36
3	3	2.195	2.184	2.207	2.193	91.08
4	5	2.129	2.107	2.127	2.121	88.00
5	7	2.093	2.069	2.107	2.095	86.93

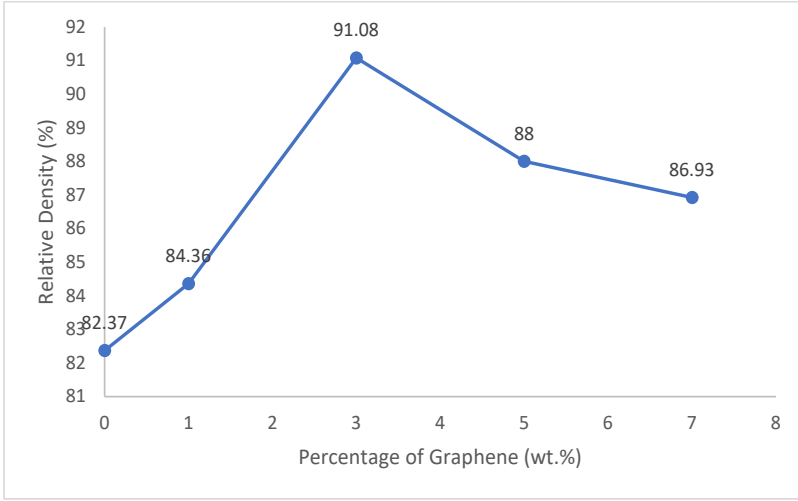

Figure 8: Relative Density (%) vs Percentage of Graphene (wt.%).

Porosity

A crucial property of biological and industrial materials is porosity. Since composites and ceramics are the most common materials used to repair injured tooth tissues, porosity is a crucial factor to take into consideration in biomaterials research [10]. The formula described in Equation (4) was used to determine the overall porosity in this study. The values of total porosity and relative density for each sample in different graphene percentages are displayed in Table 4. It indicates that the sample is less porous at high relative densities (3 wt.% of graphene and 91.08% of relative density with 8.92% porosity) and extremely porous at low relative densities (0 wt.% of graphene and 82.37% of relative density with 17.63% porosity). Higher porosity improves permeability but degrades mechanical strength [11].

Figure 9 shows a decreasing pattern in porosity as the graphene percentage increases up to 3 wt.% and then decreases at 5 wt.% and 7 wt.%. This pattern suggests that a 3 wt.% graphene composition is the optimum value as it allows a denser and more compact structure in the substance. Raising the percentage of graphene can lead to more tightly packed particles and make it easier to extract volatiles or trapped gases from the material [12]. Despite this, the dental implant may benefit from control pores. When

compared to flexible materials, control pores in dental implants, for instance, may function as a mechanism to dramatically reduce implant stiffness [13] and boost fracture toughness [14].

Table 4: Bulk density, relative density and porosity of Mg-Zn sample with vary percentage of graphene.

Sample	Graphene (wt.%)	Bulk density (g/cm³)	Relative Density (%)	Porosity (%)
1	0	1.985	82.37	17.63
2	1	2.033	84.36	15.64
3	3	2.193	91.08	8.92
4	5	2.121	88.00	12.00
5	7	2.095	86.93	13.07

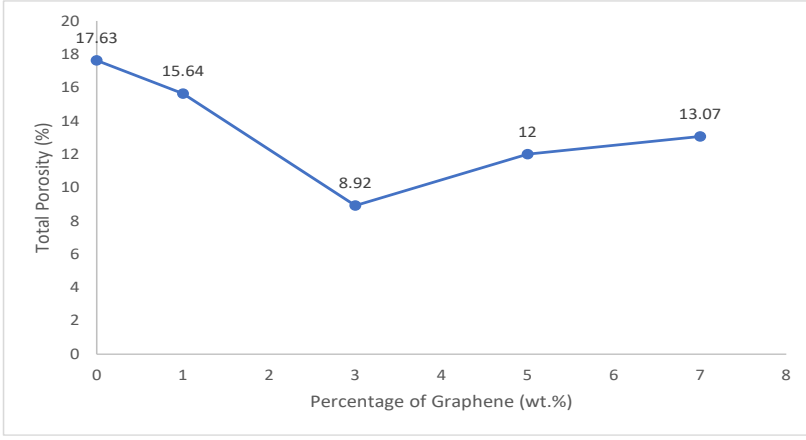

Figure 9: Graph of Total Porosity vs Percentage of Graphene (wt.%).

Rockwell Hardness Test

The data on the Rockwell hardness test for each sample in different graphene percentages is shown in Figure 10 while the average HRF value following three indentations is shown in Table 5. As the amount of graphene increases, the Rockwell hardness results show a growing trend in the graph. The highest hardness value is with addition 3 wt.% of graphene (53.93 HRF), while the lowest reading is for 0 wt.% of graphene (26.67 HRF). However, after the hardness test had been done to 3 set of samples, the

reading of Rockwell hardness test for sample with percentage of graphene 5 wt.% and 7 wt.% could not be taken because the sample had cracked and split into two during the testing process. Too much graphene could not be properly integrated into the matrix material, which would result in a weaker connection and decreased strength all around [15]. Furthermore, a key mechanical characteristic that determines whether materials, especially alloys, may be utilised for dental implants and bone [16] is hardness.

Table 5: Reading for Rockwell hardness test of Mg-Zn sample with vary percentage of graphene.

Sample	Percentage of graphene (wt.%)	Reading for Rockwell hardness test			
		1st indent	2nd indent	3rd indent	Average
1	0	27.9	25.4	26.7	26.67
2	1	41.8	43.4	45.2	43.47
3	3	52.2	55.7	53.9	53.93
4	5	0	0	0	0
5	7	0	0	0	0

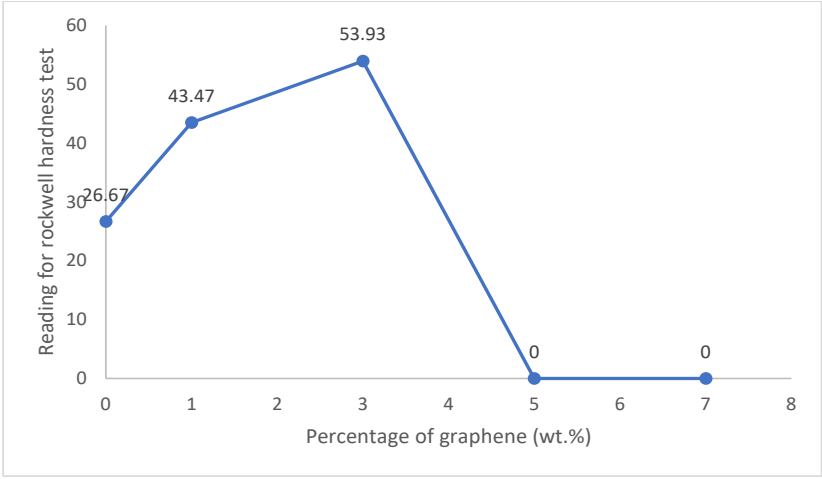

Figure 10: Graph of Reading for Rockwell hardness test vs Percentage of Graphene (wt.%).

Optical Microscope

An optical microscope (OM) was used to reveal the microstructure of graphene reinforced by Mg-Zn alloy matrix composites, as seen in Figure 11, 12, and 13. In this investigation, OM was seen for samples with percentages of graphene at 0 wt.%, 1 wt.%, and 3 wt.%. This is due to the fact that, according to the Archimedes test and the Rockwell hardness test, sample with a graphene percentage of 0 wt.% show the highest porosity and lowest density, whereas sample with a graphene percentage of 3 wt.% show the lowest porosity and maximum density. In the meantime, the Rockwell hardness test results for the 5 wt.% and 7 wt.% graphene percentages are not obtained. As a consequence, OM was applied to these samples in order to analyse the surface pores and support the outcome.

Figure 11 displays the microstructure of the sample with a 0 wt.% of graphene. Given the amount of surface cracks, the diagram indicates that the sample's surface has both open and through pores. The pattern of through, close, and blind pores that can appear in a sample is shown in Figure 11. A continuous communication channel between pores (blind and interconnected pores) and the outer surface results in an open porosity that allows for the flow of liquids and gases, along with the related processes of heat exchange, filtration, diffusion, sorption, and chemical reactions [17].

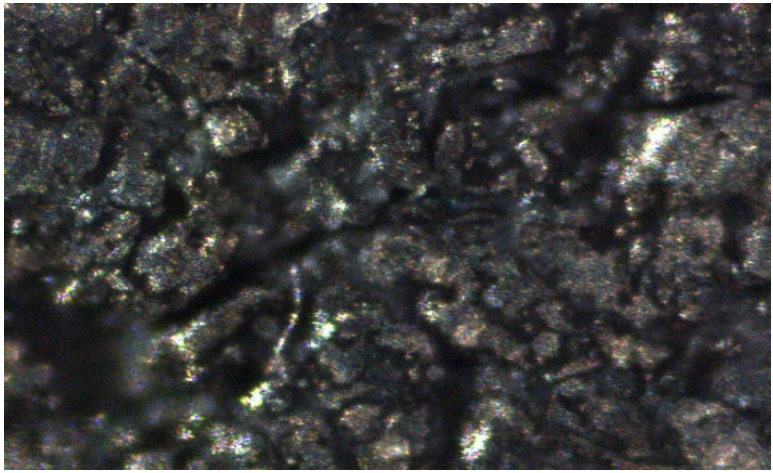

Figure 11: Surface structure of sample at percentage of graphene of 0 wt.%.

Finally, Figure 12 demonstrates that the sample with a 1 wt.% of graphene has minor fractures as opposed to a 0 wt.% of graphene. The surface structure of Mg-Zn reinforced graphene at a 3 wt.% of graphene is depicted in Figure 13. Because there are not many surface fractures, the structure seems to be less permeable than the 0 wt.% of graphene. This shows that holes or fissures on the surface vanish as the temperature rises, making the sample less fragile. But excessive polishing and ethanol usage have distorted the surface's clarity, making some phases darker and others brighter. As can be seen below, the image also shows that magnesium and zinc have a relationship. Referring to Figure 13, which illustrates the presence of the Mg-Zn phase on the metal structure, supports this assertion.

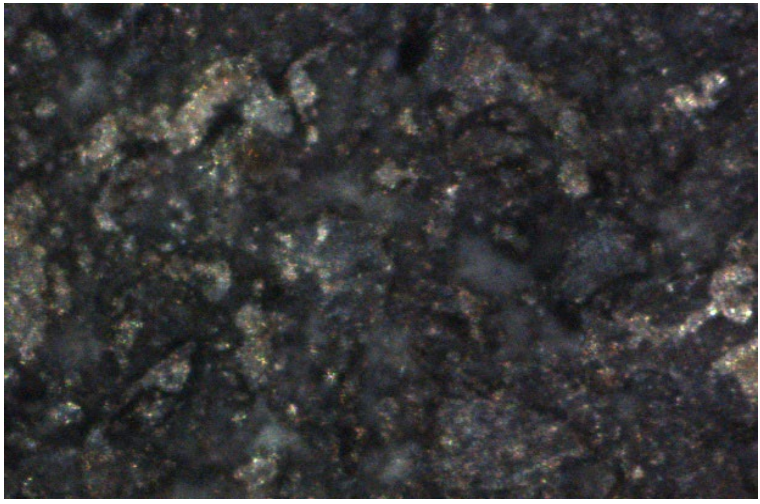

Figure 12: Surface structure of sample at percentage of graphene of 1 wt.%.

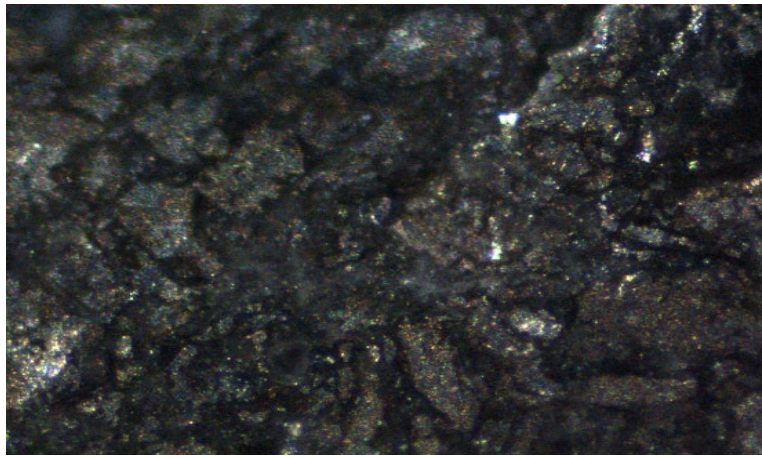

Figure 13: Surface structure of sample at percentage of graphene of 3 wt.%.

CONCLUSION

In conclusion, the research has met its primary objective to fabricate Mg-Zn reinforced with graphene using the powder metallurgy method, as well as has achieved to determine the physical and mechanical properties of Mg-Zn reinforced with graphene composites. Using powder metallurgy is an effective method for fabricating Mg-Zn matrix composites reinforced with graphene, providing greater control over pore structure and enhancing reinforcement to natural bone tissue. This study reveals that a 3 wt.% graphene content is optimal, yielding high density, low porosity, and significant strength compared to other tested percentages (0 wt.%, 1 wt.%, 5 wt.%, and 7 wt.%). The 1 wt.% graphene content is the least preferable due to its low density, high porosity, and weak matrix bonding. Specifically, the sample with 1 wt.% graphene exhibits the highest porosity (15.64%) and lowest relative density (82.37%), whereas the sample with 3 wt.% graphene shows the lowest porosity (8.92%) and highest relative density (91.08%). These findings enhance our understanding of the material's properties and highlight its potential applications in biomaterials.

ACKNOWLEDGEMENT

The authors acknowledge the Faculty of Chemical Engineering & Technology, Universiti Malaysia Perlis, Centre of Excellence for Frontier Materials Research (CFMR), Universiti Malaysia Perlis and SIG (Special Interest Group) Metal Processing & Metallurgy Research Group (MetaPrime), Universiti Malaysia Perlis for the generous collaboration in the acquisition of data and results.

REFERENCES

[1] K.S. Sridhar Raja, U. Manoj Kumar, S. Mathivanan, S. Ganesan, T. ArunKumar, J. Hemanandh & J. Senthil Kumar, 2021. Mechanical and microstructural properties of graphene reinforced magnesium composite, *Materials Today: Proceedings*, 44, 3571 – 3574.

[2] W. Xu, C. Li, Y. Zhang, H.M. Ali, S. Sharma, R. Li, M. Yang, T. Gao, M. Liu, X. Wang, Z. Said, X. Liu & Z. Zhou, 2022. Electrostatic atomization minimum quantity lubrication machining: from mechanism to application, *International Journal of Extreme Manufacturing,* 4(4), 042003.

[3] Y. Cao, V. Fatemi, S. Fang, K. Watanabe, T. Taniguchi, E. Kaxiras & P. Jarillo-Herrero, 2018. Unconventional superconductivity in magic-angle graphene superlattices, *Nature,* 556(7699), 43 – 50.

[4] A.C. Ferrari & D.M. Basko, 2013. Raman spectroscopy as a versatile tool for studying the properties of graphene, *Nature Nanotechnology,* 8(4), 235 – 246.

[5] E. Khare, N. Holten-Andersen & M. J Buehler, 2021. Transition-metal coordinate bonds for bioinspired macromolecules with tunable mechanical properties, *Nature Reviews Material*s, 6(5), 421–436.

[6] M. Rashad, F. Pan, H. Hu, M. Asif, S. Hussain, & J. She, 2015. Enhanced tensile properties of magnesium composites reinforced with graphene nanoplatelets, *Materials Science and Engineering:* A, 630,

36 – 44.

[7] K. Li, X. Wang, Y. Gao, W. Dong & H. Li., 2022. Preparation of nickel-coated graphene and evaluation of infrared interference performance, *Journal of Physics*, 2194(1), 012043.

[8] S. Xiang, X. Wang, M. Gupta, K. Wu, X. Hu & M. Zheng, 2016. Graphene nanoplatelets induced heterogeneous bimodal structural magnesium matrix composites with enhanced mechanical properties, *Scientific Reports,* 6(1).

[9] W. Ye, M. Xie, Z. Huang, H. Wang, Q. Zhou, L. Wang, B. Chen, H. Wang & W. Liu, 2023. Microstructure and tribological properties of in-situ carbide/CoCrFeNiMn high entropy alloy composites synthesized by flake powder metallurgy, *Tribology International,* 181, 108295.

[10] W. H. Kan, L. N. S. Chiu, C. V. S. Lim, Y. Zhu, Y. Tian, D. Jiang & A. Huang, 2022. A critical review on the effects of process-induced porosity on the mechanical properties of alloys fabricated by laser powder bed fusion, *Journal of Materials Science*, 57(21), 9818 – 9865.

[11] H. Liu, G. Luo, H. Wei & H. Yu, 2018. Strength, Permeability, and Freeze-Thaw Durability of Pervious Concrete with Different Aggregate Sizes, Porosities, and Water-Binder Ratios, *Applied Science*s, 8(8), 1217.

[12] L. Xiang, A. K. Darboe, Z. Luo, X. Qi, J. Shao, X. Ye, C. Liu, K. Sun, Y. Qu, J. Xu & W. Zhong, 2023. Constructing two-dimensional/two-dimensional reduced graphene oxide/MoX_2 (X = Se and S) van der Waals heterojunctions: a combined composition modulation and interface engineering strategy for microwave absorption, *Advanced Composites and Hybrid Materials*, 6(6).

[13] S. Ghouse, N. Reznikov, O.R Boughton, S. Babu, K.G. Ng, G. Blunn, J.P Cobb, M.M. Stevens & J.R. Jeffers, 2019. The design and in vivo testing of a locally stiffness-matched porous scaffold, *Applied Materials Today*, 15, 377 – 388.

[14] P. Trueba, C. Navarro, J.A. Rodríguez-Ortiz, A.M. Beltrán, F.J. García-García & Y. Torres, 2021. Fabrication and characterization of superficially modified porous dental implants, *Surface & Coatings Technology/Surface and Coatings Technology,* 408, 126796.

[15] Y. M. Wang, T. Voisin, J.T. McKeown, J. Ye, N.P. Calta, Z. Li, Z. Zeng, Y. Zhang, W. Chen, T.T. Roehling, R.T. Ott, M.K. Santala, P.J. Depond, M.J. Matthews, A.V. Hamza & T. Zhu, 2017. Additively manufactured hierarchical stainless steels with high strength and ductility, *Nature Materials*, 17(1), 63 – 71.

[16] J. Chen, P. Wu, Q. Wang, Y. Yang, S. Peng, Y. Zhou, C. Shuai & Y. Deng, 2016. Influence of alloying treatment and rapid solidification on the degradation behavior and mechanical properties of MG, *Metals,* 6(11), 259.

[17] K. Sarna-Boś, K. Skic, J. Sobieszczański, P. Boguta & R. Chałas, R., 2021. Contemporary approach to the porosity of dental materials and methods of its measurement, *International Journal of Molecular Sciences*, 22(16), 8903.